International Journal of Minerals, Metallurgy and Materials
Volume 24, Number 7, July 2017, Page 804
DOI: 10.1007/s12613-017-1464-8

Microwave absorption properties of $SiC@SiO_2@Fe_3O_4$ hybrids in the 2–18 GHz range

Peng Zhou[1)], *Jun-hong Chen*[2)], *Meng Liu*[2)], *Peng Jiang*[2)], *Bin Li*[3)], *and Xin-mei Hou*[3)]

1) National Engineering Research Center for Advanced Rolling Technology, University of Science and Technology Beijing, Beijing 100083, China
2) School of Material Science and Engineering, University of Science and Technology Beijing, Beijing 100083, China
3) Collaborative Innovation Center of Steel Technology, University of Science and Technology Beijing, Beijing 100083, China
(Received: 25 October 2016; revised: 13 March 2017; accepted: 16 March 2017)

Abstract: To enhance the microwave absorption performance of silicon carbide nanowires (SiCNWs), SiO_2 nanoshells with a thickness of approximately 2 nm and Fe_3O_4 nanoparticles were grown on the surface of SiCNWs to form $SiC@SiO_2@Fe_3O_4$ hybrids. The microwave absorption performance of the $SiC@SiO_2@Fe_3O_4$ hybrids with different thicknesses was investigated in the frequency range from 2 to 18 GHz using a free-space antenna-based system. The results indicate that $SiC@SiO_2@Fe_3O_4$ hybrids exhibit improved microwave absorption. In particular, in the case of an $SiC@SiO_2$ to iron(III) acetylacetonate mass ratio of 1:3, the microwave absorption with an absorber of 2-mm thickness exhibited a minimum reflection loss of −39.58 dB at 12.24 GHz. With respect to the enhanced microwave absorption mechanism, the Fe_3O_4 nanoparticles coated on $SiC@SiO_2$ nanowires are proposed to balance the permeability and permittivity of the materials, contributing to the microwave attenuation.

Keywords: silicon carbide nanowires; hybrids; microwave absorption; mechanism; impedance match

1. Introduction

Electromagnetic (EM) pollution by electronic devices and communications equipment has increased interest in investigations of microwave-absorbing materials [1–2]. However, existing absorbing materials often have shortcomings such as high density, a large matching thickness and a narrow absorption band. Efficient microwave absorbers with low weight, good thermal stability, a wide absorption frequency range, and high absorption capability are highly desirable and necessary [3–5]. Silicon carbide (SiC) nanostructures are highly desirable as EM absorbers because of their excellent strength, low density, chemical inertness and good dielectric loss to microwave radiation [6–7]. Compared with other carbon materials, SiC can be used under high-temperature conditions and its loss factor increases with temperature [8–9]. One-dimensional SiC nanowires have been found to possess substantially higher permittivity than SiC nanoparticles [6]. Furthermore, the criteria of being lightweight, thin and absorbing microwaves over a broad frequency bandwidth can be realized by SiC. However, the EM parameters of pure SiC do not satisfy the requirement of impedance matching, which results in strong reflection and weak absorption.

Current microwave absorption research tends to be heavily focused on ferrite-based materials, metal powders, related alloys, and various newly developed nanosized materials because they produce large electric, magnetic, and/or dielectric losses [10]. However, ferrites' intrinsic disadvantages of high density and low strength restrict their widespread application. In addition, their absorption bandwidth is relatively narrow and their magnetic characteristics are lost above the Curie temperature [11].

Fabricating composites by combining low-density dielectric loss materials with strong absorption magnetic loss absorbing materials has been demonstrated as an effective approach to improving the EM-wave absorption ability. Kong *et al.* [12] synthesized γ-Fe_2O_3/reduced graphene

Corresponding author: Xin-mei Hou E-mail: houxinmeiustb@ustb.edu.cn

oxide (RGO) hybrids via a solvothermal method. γ-Fe_2O_3 colloidal nanoparticle clusters were assembled on RGO sheets, which led to effective optimization of EM parameters. This special construction can ensure impedance matching; thus, the material exhibits strong absorbing capability [13]. Fe_3O_4 is well known to exhibit high chemical stability and a high Curie temperature [14], which suggests that a composite containing Fe_3O_4 might exhibit enhanced microwave absorption.

With respect to the fabrication of hybrid materials, the interface characteristics are also important. SiC is well known to exhibit weak hydrophilicity, with a water contact angle of approximately 75°. Such poor wettability limits the excellent performance of SiC when it is used in composites [15]. In our recent work, SiO_2-coating-modified SiC nanowires displayed good hydrophilicity because of a large number of silanol groups formed on the surface of the SiO_2 shells as well as in the interspace between nanowires [16]. In this work, $SiC@SiO_2@Fe_3O_4$ hybrids were produced using a convenient polyol approach. The hybrids show improved microwave absorption compared to pure SiC nanowires. The mechanism of this enhancement is discussed.

2. Experimental

2.1. Materials

Gangue (SiO_2, purity > 99%), carbon black, iron(III) acetylacetonate ($Fe(acac)_3$), ethyl acetate, and sodium hydroxide were supplied by Sinopharm Chemical Reagent Beijing Co., Ltd. Argon (99.99%) was supplied by Haipu Gas Co., Ltd. Deionized water and ethanol were used in all of the experiments.

2.2. Synthesis of $SiC@SiO_2@Fe_3O_4$ hybrids

$SiC@SiO_2$ nanowires were produced on a large scale through carbothermal reduction methods using gangue and carbon black as the raw materials [17]. The prepared gray nanowires were treated in an alkaline solution of 1 mol/L NaOH for 1 h to form an ultra-thin SiO_2 shell on the surface; NaOH solution facilitates the formation of Si–O–Fe bonds and prevents the aggregation of Fe_3O_4 nanoparticles [18]. The preparation procedure of $SiC@SiO_2@Fe_3O_4$ hybrids was as follows: 100 mg $SiC@SiO_2$ nanowires were added to 25 mL triethylene glycol solution in an ultrasonic bath to obtain a uniform suspension. The iron precursor, $Fe(acac)_3$, was added to the resulting suspension, and the resulting mixture was sonicated for approximately 30 min to form a well-distributed solution. The mixture was subsequently heated to 280°C at a rate of 3°C·min^{-1} under vigorous stirring and argon protection. After cooling to room temperature, 30 mL of ethyl acetate was added to dilute the solution. Finally, the products were magnetically separated, washed with ethanol and deionized water several times and dried in a vacuum oven. To investigate the effect of the Fe_3O_4 content on the microwave absorption performance, different mass ratios of $SiC@SiO_2$ to $Fe(acac)_3$, i.e., 1:1, 1:2, 1:3, and 1:4, were prepared.

2.3. Characterization

The phases were identified by X-ray diffraction (XRD) using Cu K_α radiation (40 kV, 20 mA, λ = 0.15406 nm) in the angular range from 10° to 80° at a scan speed of 2°/min. Fourier transform infrared (FT-IR) spectra were recorded in transmission mode in the spectral scanning range from 2000 to 500 cm^{-1} using a Nicolet-Nexus 470 infrared spectrophotometer. Raman spectra were recorded on an ALMEGA confocal laser micro-Raman spectrometer using Ar-ion laser excitation with a wavelength of 325 nm. X-ray photoelectron spectroscopy (XPS) was performed on a VG Multilab 2009 system. The morphologies of the products were examined by field-emission scanning electron microscopy (SEM; FEI-SIRION, operated at 5 kV). Transmission electron microscopy (TEM) with high-resolution transmission electron microscopy (HRTEM) and selected-area electron diffraction (SAED) were performed on a Tecnai G2 F30 S-TWIN. Magnetic measurements were carried out using a physical property measurement system (PPMS; Quantum Design, PPMS-9).

The relative complex permittivity and permeability as functions of frequency were obtained by the coaxial reflection/transmission method using an Agilent E8363A vector network analyzer in the frequency range from 2 to 18 GHz. The samples for measurement were prepared by milling 50wt% of the samples in a paraffin wax matrix and the experiment was carried out at 50°C. For the test, the obtained mixture was molded into a ring with a 3-mm interior diameter, 7-mm exterior diameter, and 2-mm height. The electromagnetic parameters of the paraffin matrixes filled with samples were investigated by measuring relative complex permittivity, $\varepsilon_r = \varepsilon' + \varepsilon''$, and permeability, $\mu_r = \mu' + \mu''$, in the frequency range from 2 to 18 GHz. Here the real relative complex permittivity (ε') and the imaginary part (ε'') of the relative complex permittivity represent the energy storage ability and loss ability, respectively. μ' and μ'' are defined as the real and imaginary parts of the relative complex permeability, respectively. The tangent of dielectric loss (δ_e) and the tangent of magnetic loss (δ_m) can be expressed as $\tan\delta_e = \varepsilon''/\varepsilon'$ and

$\tan\delta_m = \mu''/\mu'$, respectively [19]. Through a combination of network analysis and transmission line theory [20–21], electromagnetic parameters such as complex permittivity and permeability can be measured.

3. Results and discussion

3.1. Phase and morphology characterization

The phase of SiC@SiO_2@Fe_3O_4 hybrids was characterized by XRD, as shown in Fig. 1. For comparison, SiC@SiO_2 nanowires synthesized in our previous work were also investigated [22]. The major peaks at 2θ = 35.7°, 41.5°, 60.1°, 71.9°, and 75.7° are indexed as the (111), (200), (220), (311), and (222) reflections of SiC (JCPDS card no. 96-101-1032), respectively. A weak broad peak at approximately 22°, which corresponds to the amorphous SiO_2 shells, was observed at high magnification after the NaOH treatment [23]. The SiO_2 shell plays a key role in the formation of SiC@SiO_2@Fe_3O_4 nanohybrids [24]. After surface modification by Fe_3O_4, new peaks at 2θ = 30.1°, 35.5°, 43.1°, 53.5°, 57.1°, and 62.7° appear; these peaks correspond to the (220), (311), (400), (422), (511), and (440) planes of the cubic spinel structure of Fe_3O_4 (JCPDS card no. 96-210-1927), respectively. The relative intensity of Fe_3O_4 became more distinct with increasing Fe_3O_4 content [25]. No other peaks were observed, indicating that SiC@SiO_2@Fe_3O_4 nanohybrids were pure.

To obtain detailed information about the structure of the synthesized products, typical SEM and TEM images were collected. Figs. 2(a) and 2(b) represent the SEM images of SiC@SiO_2 nanowires at low and high magnifications, respectively. The nanowires can be characterized as long and straight filaments possessing smooth surface with a length up to several millimeters. The TEM image (Fig. 2(c)) shows that the nanowires have a core–shell structure. The corresponding SAED pattern in the inset of Fig. 2(c) indicates that the silica layer is amorphous and that the thickness is approximately 2 nm. After the Fe_3O_4 modification on the surface, if we take the SiC@SiO_2@Fe_3O_4 hybrids with an SiC@SiO_2-to-Fe(acac)$_3$ mass ratio of 1:3 as an example, the surface becomes extremely rough (Figs. 2(d) and 2(e)). HRTEM analysis (Fig. 2(f)) indicates that two types of lattice fringes corresponding to the (111) plane of SiC and the (311) plane of Fe_3O_4 are observed. This result

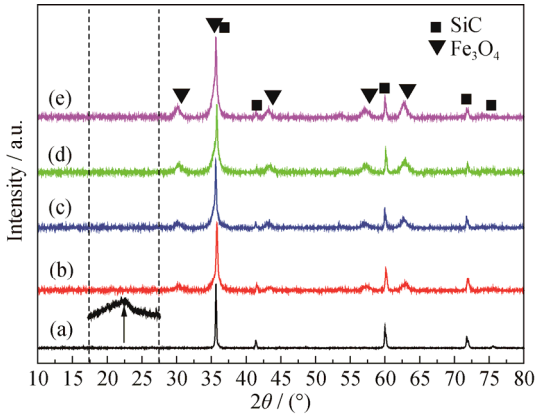

Fig. 1. XRD patterns of SiC@SiO_2 nanowires (a) and SiC@SiO_2@Fe_3O_4 with SiC@SiO_2 to Fe(acac)$_3$ mass ratios of 1:1 (b), 1:2 (c), 1:3 (d), and 1:4 (e). The arrow inset shows the magnification part at about 22°.

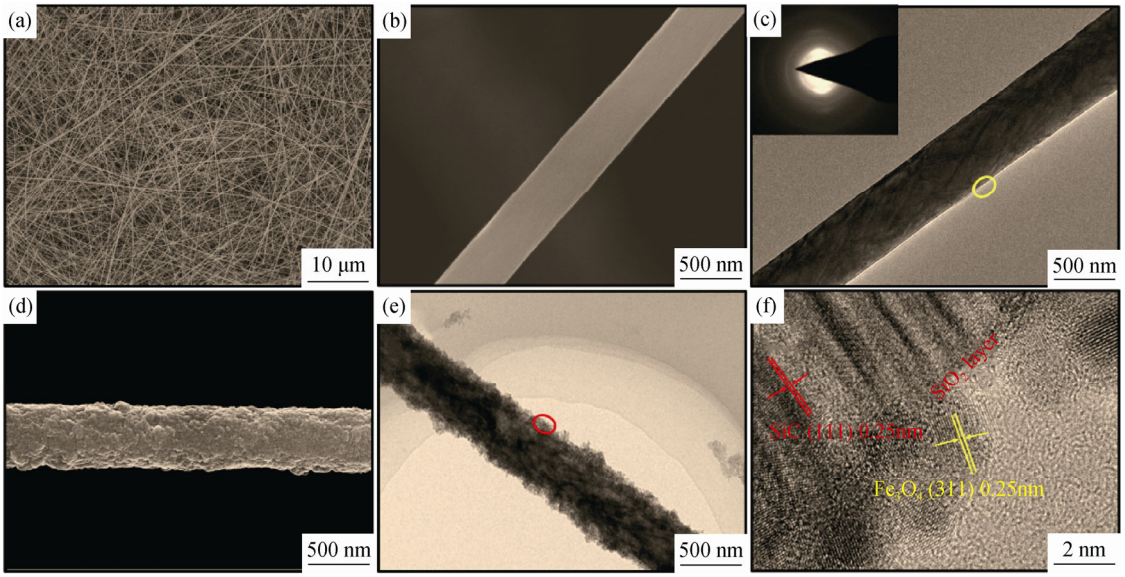

Fig. 2. SEM (a,b) and TEM (c) images of SiC@SiO_2 nanowires; SEM (d) and TEM (e,f) images of SiC@SiO_2@Fe_3O_4 hybrids with an SiC@SiO_2-to-Fe(acac)$_3$ mass ratio of 1:3.

is in agreement with the XRD analysis (Fig. 1). The thickness of Fe_3O_4 is approximately 5 nm and it is uniformly distributed on the surface. The silica layer is also present, as shown in Fig. 2(f). Even after sonication for an extended period, Fe_3O_4 nanoparticles remain firmly and uniformly anchored onto the surface of SiC@SiO_2 nanowires, indicating the strong interaction between the two substances.

To further investigate the phase structure of SiC@SiO_2 nanowires and SiC@SiO_2@Fe_3O_4 hybrids, FT-IR was carried out, as shown in Fig. 3. The strong bands at 800.99 and 926.50 cm^{-1} correspond to stretching vibrations of the Si–C bonds [26]. The peak at 1107.19 cm^{-1} corresponds to an Si–O antisymmetric stretching frequency and is attributed to the amorphous silica on the surface [27]. After the Fe_3O_4 coating was applied, a peak at 583.09 cm^{-1} corresponding to an Fe–O vibration appears in the spectrum; this vibration likely originates from Fe_3O_4 nanoparticles. Collectively, these spectral results indicate that SiC@SiO_2@Fe_3O_4 hybrids were successfully synthesized. The absorption band at 1622.4 cm^{-1} is attributed to Si−OH groups in the sample [28].

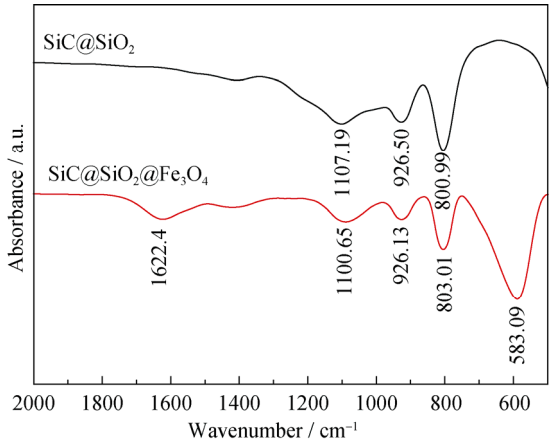

Fig. 3. FT-IR spectra of SiC@SiO_2 nanowires and SiC@SiO_2@Fe_3O_4 hybrids.

Fig. 4 shows the Raman spectra of the as-prepared SiC@SiO_2@Fe_3O_4 hybrids. In the case of small amounts of coated Fe_3O_4 nanoparticles, two intense peaks are observed at 790 and 950 cm^{-1}; these peaks correspond to the transverse phonon (TO) mode and the longitudinal optical (LO) mode of SiC, respectively. The peaks at 1353 and 1580 cm^{-1} are both related to sp^3 C and sp^2 C, which may arise from defects in the SiC structure. With increasing amount of Fe_3O_4, the LO mode of SiC at 958 cm^{-1} gradually weakens and almost disappears. A similar phenomenon occurs in the cases of the peaks at 1353 and 1580 cm^{-1}. By comparison, the intensity of the peak at 680 cm^{-1}, which is the typical characteristic peak of Fe_3O_4, gradually increases, further confirming that SiC@SiO_2@Fe_3O_4 hybrids were successfully synthesized [29–30]. The increase in intensity of Fe_3O_4 peaks and decrease in intensity of SiC peaks suggest an increase in the amount of Fe_3O_4 nanoparticles.

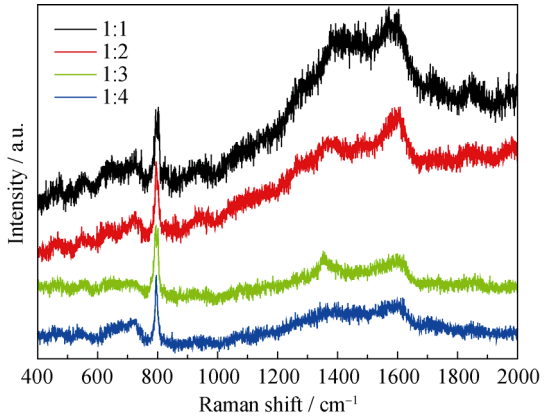

Fig. 4. Raman spectra of SiC@SiO_2@Fe_3O_4 hybrids with SiC@SiO_2-to-Fe(acac)$_3$ mass ratios of 1:1, 1:2, 1:3, and 1:4.

Structural information about the synthesized SiC@SiO_2 and SiC@SiO_2@Fe_3O_4 was analyzed by XPS; the corresponding results are shown in Fig. 5. Compared with the XPS spectrum of SiC@SiO_2 (Fig. 5(a)), that of the SiC@SiO_2@Fe_3O_4 hybrid shows an emergent signal corresponding to the characteristic peak of Fe. The two Fe peaks with binding energies of 710.8 and 724.4 eV in the high-resolution Fe 2p spectrum (Fig. 5(b)) are attributed to Fe $2p_{3/2}$ and Fe $2p_{1/2}$ of trivalent Fe in the Fe_3O_4 [31–32]. In addition, the peak at 530.6 eV is attributed to O 1s; its intensity increases significantly after modification, indicating that Fe_3O_4 was successfully formed on the SiC@SiO_2 surface. The peak at 284.5 eV is attributed to C 1s. The peaks at 151.7 and 100.8 eV are assigned to Si 2s and Si 2p of SiC@SiO_2 [33]. Moreover, the intensities of the peaks of C and Si decrease substantially with increasing amount of Fe_3O_4, which is attributable to the fact that SiC@SiO_2 was almost fully covered by Fe_3O_4 nanoparticles.

The field-dependent magnetization curves of SiC@SiO_2@Fe_3O_4 nanohybrids were also measured at room temperature, as shown in Fig. 6. The Fe_3O_4 nanoparticles endow the SiC@SiO_2@Fe_3O_4 hybrids with ferromagnetism. The saturation magnetization and coercivity were measured to be 13.42, 23.20, 32.64, 43.97 emu·g^{-1} and 31.34, 26.21, 32.45, 34.64 Oe, corresponding to SiC@SiO_2-to-Fe(acac)$_3$ mass ratios of 1:1, 1:2, 1:3, and 1:4, respectively. Magnetic Fe_3O_4 nanoparticles contribute to magnetic loss to an EM wave, which results in effective wave-absorbing perfor-

mance [34].

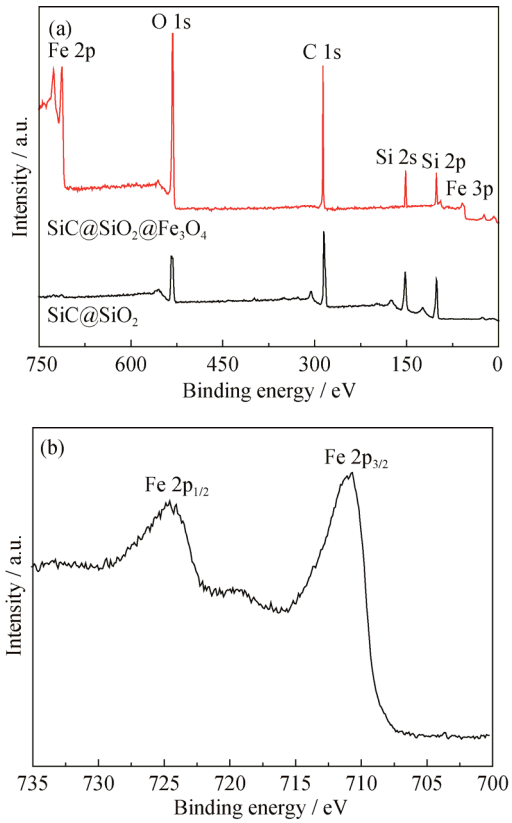

Fig. 5. Full XPS spectra of SiC@SiO_2 and SiC@SiO_2@Fe_3O_4 hybrids (a) and Fe 2p of SiC@SiO_2@Fe_3O_4 hybrids (b).

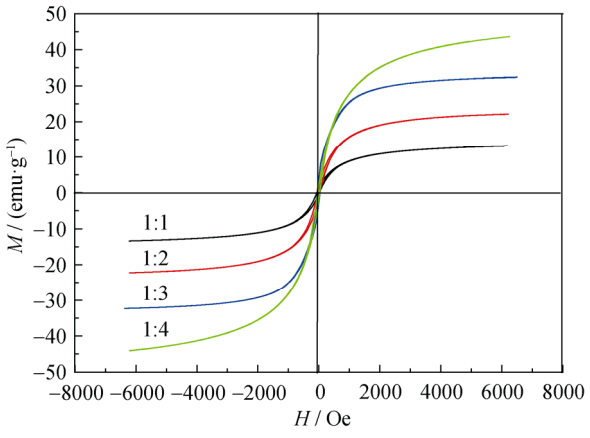

Fig. 6. Magnetic hysteresis loops of SiC@SiO_2@Fe_3O_4 hybrids with SiC@SiO_2-to-Fe(acac)$_3$ mass ratios of 1:1, 1:2, 1:3, and 1:4.

3.2. Microwave absorption performance

Fig. 7 presents the real part ε' and imaginary part ε'' of the complex relative permittivity and the dielectric tangent loss $\tan\delta_e$ of SiC@SiO_2 nanowires and SiC@SiO_2@Fe_3O_4 hybrids in the frequency range from 2 to 18 GHz. Compared with the microwave absorption performance of SiC@SiO_2 nanowires, the values of the complex relative permittivity (ε', ε'') and dielectric tangent loss $\tan\delta_e$ of SiC@SiO_2@Fe_3O_4 hybrids increase. In addition, the value of $\tan\delta_e$ for the sample with an SiC@SiO_2-to-Fe(acac)$_3$ mass ratio of 1:3 is the highest. Notably, in the case of the sample with an SiC@SiO_2-to-Fe(acac)$_3$ mass ratio of 1:1, a sharp shoulder peak appears at the frequency of 15 GHz. This peak is attributed to the presence of fewer coated Fe_3O_4 nanoparticles because they well balance the permeability and permittivity of the materials by making their EM impedances match. Thus, most of the EM waves are able to transmit into the materials. The microwaves in the materials are intensively attenuated, which leads to a lower EM reflection. The minimum reflection loss of an EM wave reaches −16.54 dB at 15 GHz, and the absorption bandwidth reaches 3 GHz in the case of an absorber with a thickness in the 1.5-mm range. In the case of an SiC@SiO_2-to-Fe(acac)$_3$ mass ratio of 1:4, no dual-loss peaks are observed, which is attributed mainly to the fact that SiC@SiO_2 is almost fully covered by Fe_3O_4 nanoparticles. The microwave absorption performance of the hybrids mainly arises from the dielectric loss of Fe_3O_4, and attaining an impedance match is difficult. Therefore, the hybrids with a thickness in the 1.5-mm range have no effective absorption band. Given that SiC is a typical dielectric material, Fe_3O_4 exhibits dual-loss characteristics. The dipole polarization presented by Fe_3O_4 nanoparticles, which mainly results from the natural physical properties of Fe_3O_4, can contribute to the dielectric loss. Dipoles are present in Fe_3O_4, especially when the particle size is nanoscale. The number of surface atoms with unsaturated bonds greatly increases as the size decreases, resulting in an increase of the number of dipoles [35]. In this work, the size of Fe_3O_4 nanoparticles was approximately 5 nm, as characterized in Fig. 2; thus, a large number of dipoles exist. A greater number of dipoles results in a higher dielectric constant. Under the external alternating electric field, the reorientation of dipoles results in polarization and energy dissipation. In this case, a high relative dielectric constant means high dielectric loss because the reorientation must be completed by the migration of ions, which dissipates energy [36]. What is more, the dielectric loss is related to the natural structure of Fe_3O_4. Its chemical formula can be written as $Fe_A^{3+}[Fe^{2+},Fe^{3+}]_BO_4^{2-}$, where Fe cations occupy interstices of a face-centered cubic closed-packed frame of oxygen ions, and A and B denote the tetrahedral sites and octahedral sites, respectively. Electrons can transfer between Fe^{2+} and Fe^{3+} ions in B sites as the field (EM wave) is applied. Therefore,

the electronic spin and charge polarization strongly affect the loss [37–38]. Based on the aforementioned analyzes, the higher dielectric loss is related to the dipole polarization presented by Fe_3O_4 nanoparticles and its natural structures. In addition to these, the interfacial polarization and the related relaxation may also improve the dielectric loss [39].

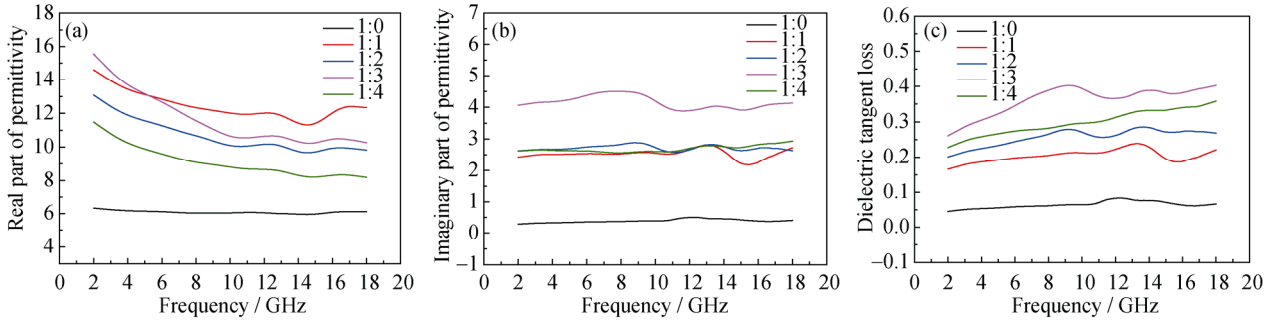

Fig. 7. Real part of the complex permittivity spectra (a), and imaginary part of the complex permittivity spectra (b), and dielectric tangential loss (c) of the SiC@SiO_2 nanowires and SiC@SiO_2@Fe_3O_4 hybrids with SiC@SiO_2-to-Fe(acac)$_3$ mass ratios of 1:0, 1:1, 1:2, 1:3, and 1:4.

Fig. 8 presents the real part μ' and imaginary part μ'' of the complex relative permeability and the magnetic tangent loss $\tan\delta_m$ of the SiC@SiO_2@Fe_3O_4 hybrids in the frequency range from 2 to 18 GHz. The values of imaginary part μ'' and magnetic tangent loss $\tan\delta_m$ increased after Fe_3O_4 nanoparticles were coated in the low-frequency region from 2 to 10 GHz, indicating that the magnetic loss mainly occurred in the low-frequency range [40]. By comparison, the value of the magnetic loss $\tan\delta_m$ was the highest when the SiC@SiO_2-to-Fe(acac)$_3$ mass ratio was 1:4. This result is attributed to the increasing content of Fe_3O_4 nanoparticles.

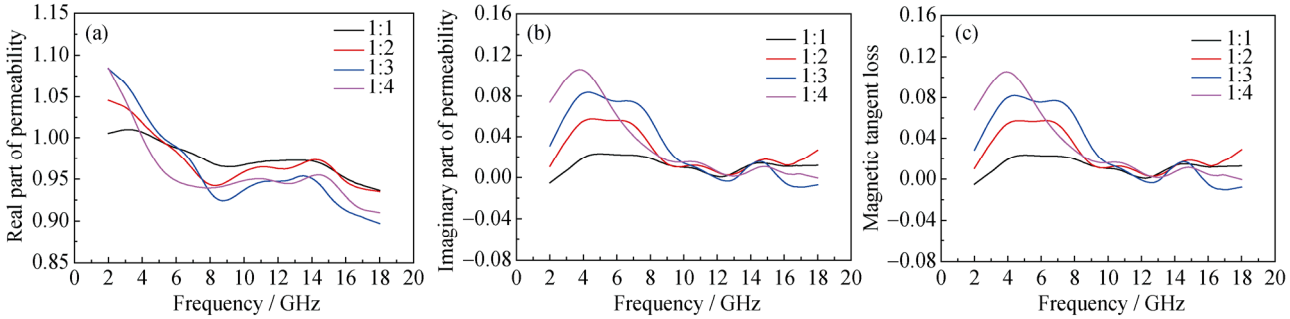

Fig. 8. Real part of the complex permeability spectra (a), imaginary part of the complex permeability spectra (b), and the magnetic tangential loss (c) of the SiC@SiO_2@Fe_3O_4 hybrids with SiC@SiO_2-to-Fe(acac)$_3$ mass ratios of 1:1, 1:2, 1:3, and 1:4.

Based on the transmission line theory [41], the reflection loss (RL, dB) of a sample is determined according to the following equations:

$$Z_{in} = Z_0(\mu_r / \varepsilon_r)^{1/2} \tanh\left[j(2\pi fd / c)(\mu_r / \varepsilon_r)^{1/2} \right] \quad (1)$$

$$RL = 20\lg\left|\frac{Z_{in} - Z_0}{Z_{in} + Z_0}\right| \quad (2)$$

where Z_{in} is the input impedance of the absorber; Z_0 is the impedance of air; μ_r and ε_r are the relative complex permeability and permittivity of the absorber, respectively; f is the frequency of the EM waves; d is the thickness of the absorber, c is the velocity of EM waves in free space, and j is the imaginary unit. When RL is smaller than −10 dB, only 10% of the microwave energy is reflected, whereas its 90% is absorbed. The corresponding frequency range, in which the RL is smaller than −10 dB, is defined as the effective absorption bandwidth.

The EM absorption performance of SiC@SiO_2 nanowires and SiC@SiO_2@Fe_3O_4 hybrids is compared in Fig. 9. The EM absorption performance was substantially enhanced after Fe_3O_4 nanoparticles were attached to the SiC@SiO_2 nanowires. The values of the reflection losses of SiC@SiO_2@Fe_3O_4 hybrids with different SiC@SiO_2-to-Fe(acac)$_3$ mass ratios were obtained to be −16.54 (1:1), −21.04 (1:2), −39.58 (1:3), and −26.54 dB (1:4) at 15.44, 6.8, 12.24, and 4.56 GHz, respectively. The optimum state for SiC@SiO_2@Fe_3O_4 hybrids to attenuate microwaves was obtained when the mass ratio between SiC@SiO_2 nanowires and Fe(acac)$_3$ was 1:3. This ratio may well result in balanced permeability and

permittivity of the material by making the microwave impedance match. Most of the microwaves are thus able to be transmitted into the material. The absorption bandwidth with the reflection loss below −10 dB is as high as 3.68 GHz (from 10.8 to 14.48 GHz) for the absorber with a thickness in the 2.0-mm range. Table 1 summarizes the EM absorption properties for typical related materials [42–46], which reveals that the effective absorption bandwidth in this work is wider while the thickness is much smaller, indicating that the SiC@SiO_2@Fe_3O_4 hybrids synthesized in this work are very promising EM-wave absorptive candidates.

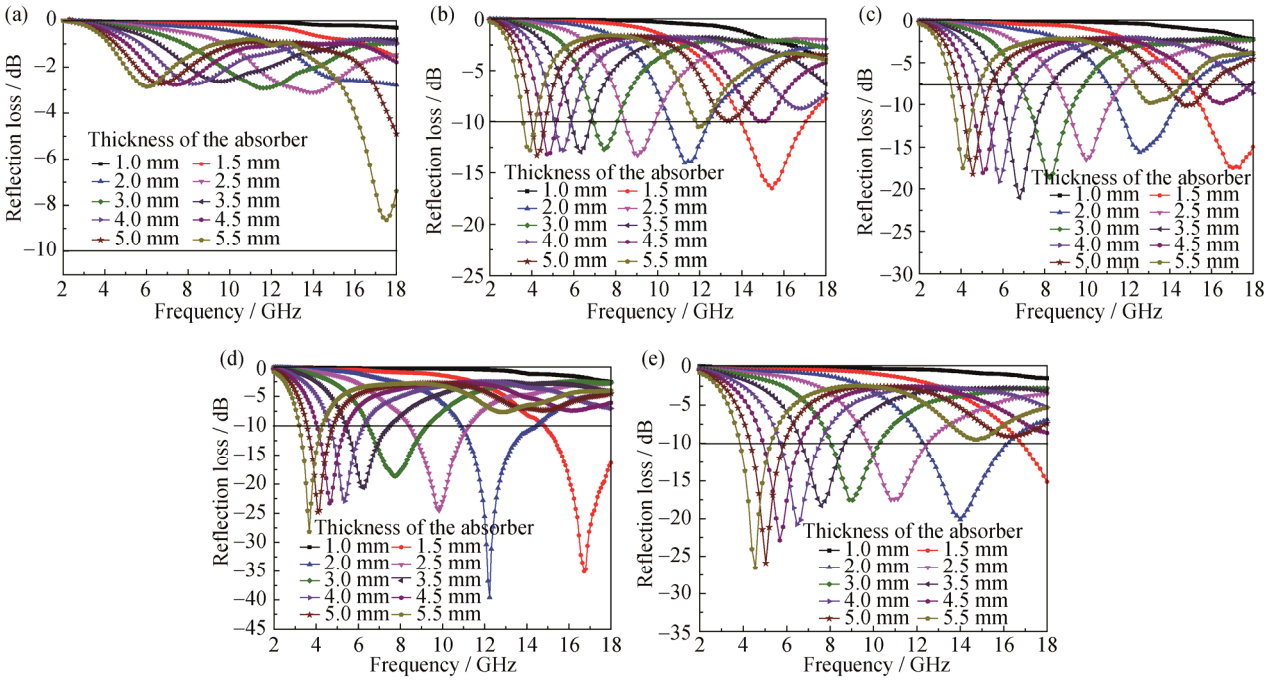

Fig. 9. Calculated reflection loss of SiC@SiO_2 nanowires (a) and SiC@SiO_2@Fe_3O_4 hybrids synthesized with SiC@SiO_2 nanowires-to-Fe(acac)$_3$ mass ratios of 1:1 (b), 1:2 (c), 1:3 (d), and 1:4 (e).

Table 1. Comparison of the microwave absorption performance of typical related materials

Sample	Minimum RL / dB	Frequency range / GHz (RL < −10 dB)	d_m / mm	Percentage of absorber / wt%	Ref.
SiC	−17.4	9.7–12.2	3.0	30	[42]
NiO@SiC	−46.9	8.2–12.4	2.0	50	[43]
CNT/SiC	−37.6	12.4–17.5	2.0	20	[44]
Fe_3O_4/Ppy/CNT	−25.9	7.8–12.5	3.0	20	[45]
Fe_3O_4@ZnO	−22.7	10.1–16.0	3.5	50	[46]
SiC@SiO_2@Fe_3O_4 hybrids in this work	−39.6	10.8–14.5	2.0	50	This work

Note: The d_m is the effective absorption bandwidth when RL is smaller than −10 dB.

In view of the improved EM wave attenuation performance of SiC@SiO_2@Fe_3O_4 hybrids, such excellent performance resulted from the natural physical properties of SiC@SiO_2 and Fe_3O_4 and the special core/shell structures. There are usually two factors for achieving a low RL value: the incident microwave should transmit into the materials with minimum reflection, and the materials should effectively attenuate the incident microwave [47]. The impedance match between the material and free space is important. This requires that the permittivity and permeability are equal in both the imaginary and the real parts. SiC attenuates microwaves by dielectric loss, which mainly originates from electronic polarization, atomic polarization and intrinsic electric dipole polarization. Fe_3O_4 exhibits dual-loss characteristics: it attenuates microwaves by both dielectric and magnetic losses, where the magnetic loss mainly originates from eddy current loss and hysteresis loss. The dipole polarization exhibited by Fe_3O_4 nanopar-

ticles contributes to the dielectric loss. Especially under an external alternating electric field, the reorientation of dipoles results in polarization and energy dissipation because the reorientation must be completed by the migration of ions, which dissipates energy [36]. In addition, the special core/shell structure of $SiC@SiO_2@Fe_3O_4$ hybrids plays a vital role in absorbing EM. The interfaces at the core and the shell are clearly observed in the HRTEM image in Fig. 2(c). The interfacial polarization and associated relaxation also contribute to the microwave attenuation [39]. Such improved dielectric loss induced by the interfacial polarization has been observed in other core/shell systems. For example, Ag–Ni core–shell materials showed additional absorption compared to the naked Ni nanoparticles, where the additional absorption was induced by the interfacial polarization [48]. Furthermore, the defects formed at the interfaces due to the crystal mismatch between SiC and SiO_2 can also serve as polarized centers, leading to an additional dielectric loss. A schematic of the possible EM absorption mechanism for hybrids is shown in Fig. 10. The Fe_3O_4 nanoparticles increase the permeability of the complex. Hybrids combine the dielectric loss of $SiC@SiO_2$ nanowires with the magnetic loss of Fe_3O_4, which may well balance the permeability and permittivity of the materials, making the EM impedance match. Therefore, most of the EM waves can be transmitted into the materials and the microwaves in the materials are intensively attenuated.

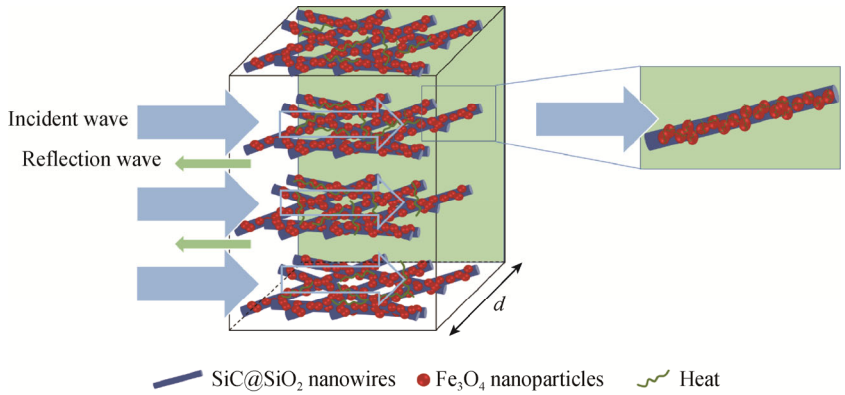

Fig. 10. Schematic of a possible EM absorption mechanism for the $SiC@SiO_2@Fe_3O_4$ hybrids.

4. Conclusions

$SiC@SiO_2@Fe_3O_4$ hybrids were successfully produced using a convenient polyol approach. Microstructural analysis revealed that Fe_3O_4 nanocrystals were immobilized onto the $SiC@SiO_2$ nanowires surface by a strong interaction. The microwave absorption performance was enhanced with the minimum reflection loss of −39.58 dB at 12.24 GHz. In particular, the $SiC@SiO_2@Fe_3O_4$ hybrids with an $SiC@SiO_2$ nanowires-to-$Fe(acac)_3$ mass ratio of 1:3 achieved an absorption bandwidth as high as 3.68 GHz (from 10.8 to 14.48 GHz) with a reflection loss below −10 dB for the absorber with a thickness in the 2.0-mm range. The main mechanism was that nanohybrids combined the dielectric loss of $SiC@SiO_2$ nanowires with the magnetic loss of Fe_3O_4, which may have well balanced the permeability and permittivity of the materials, making the EM impedance match.

Acknowledgements

This work was financially supported by the National Science Fund for Excellent Young Scholars of China (No. 51522402), the National Natural Science Foundation of China (Nos. 51572019 and U1460201), and the Fundamental Research Funds for the Central Universities (No. FRF-TP-15-006C1).

References

[1] M. Yu, C.Y. Liang, M.M. Liu, X.L. Liu, K.P. Yuan, H. Cao, and R.C. Che, Yolk–shell $Fe_3O_4@ZrO_2$ prepared by a tunable polymer surfactant assisted sol–gel method for high temperature stable microwave absorption, *J. Mater. Chem. C*, 2(2014), p. 7275.

[2] H. Sun, R.H. Che, X. You, Y.S. Jiang, Z.B. Yang, J. Deng, L.B. Qiu, and H.S. Peng, Cross-stacking aligned car-

bon-nanotube films to tune microwave absorption frequencies and increase absorption intensities, *Adv. Mater.*, 26(2014), No. 48, p. 8120.

[3] W.L. Song, M.S. Cao, L.Z. Fan, M.M. Lu, Y. Li, C.Y. Wang, and H.F. Ju, Highly ordered porous carbon/wax composites for effective electromagnetic attenuation and shielding, *Carbon*, 77(2014), p. 130.

[4] E. Vázquez and M. Prato, Carbon nanotubes and microwaves: interactions, responses, and applications, *ACS Nano*, 3(2009), No. 12, p. 3819.

[5] W.L. Song, X.T. Guan, L.Z. Fan, Y.B. Zhao, W.Q. Cao, C.Y. Wang, and M.S. Cao, Strong and thermostable polymeric graphene/silica textile for lightweight practical microwave absorption composites, *Carbon*, 100(2016), p. 109.

[6] J.L. Kuang and W.B. Cao, Silicon carbide whiskers: preparation and high dielectric permittivity, *J. Am. Ceram. Soc.*, 96(2013), p. 2877.

[7] S.L. Chen, P.Z. Ying, L. Wang, G.D. Wei, F.M. Gao, J.J. Zheng, M.H. Shang, Z.B. Yang, W.Y. Yang, and T. Wu, Highly flexible and robust N-doped SiC nanoneedle field emitters, *NPG Asia Mater.*, 7(2015), p. e157.

[8] H.J. Yang, J. Yuan, Y. Li, Z.L. Hou, H.B. Jin, X.Y. Fang, and M.S. Cao, Silicon carbide powders: temperature-dependent dielectric properties and enhanced microwave absorption at gigahertz range, *Solid State Commun.*, 163(2013), p. 1.

[9] M.S. Cao, W.L. Song, Z.L. Hou, B. Wen, and J. Yuan, The effects of temperature and frequency on the dielectric properties, electromagnetic interference shielding and microwave-absorption of short carbon fiber/silica composites, *Carbon*, 48(2010), No. 3, p. 788.

[10] L.B. Kong, Z.W. Li, L. Liu, R. Huang, M. Abshinova, Z.H. Yang, C.B. Tang, P.K. Tan, C.R. Deng, and S. Matitsine, Recent progress in some composite materials and structures for specific electromagnetic applications, *Int. Mater. Rev.*, 58(2013), No. 4, p. 203.

[11] X.W. Yin, L. Kong, L.T. Zhang, L.F. Cheng, N. Travitzky, and P. Greil, Electromagnetic properties of Si–C–N based ceramics and composites, *Int. Mater. Rev.*, 59(2014), No. 6, p. 326.

[12] L. Kong, X.W. Yin, Y.J. Zhang, X.Y. Yuan, Q. Li, F. Ye, L.F. Cheng, and L.T. Zhang, Electromagnetic wave absorption properties of reduced graphene oxide modified by maghemite colloidal nanoparticle clusters, *J. Phys. Chem. C*, 117(2013), No. 38, p. 19701.

[13] W.Y. Duan, X.W. Yin, F. Ye, Q. Li, M.K. Han, X.F. Liu, and Y.Z. Cai, Synthesis and EMW absorbing properties of nano SiC modified PDC–SiOC, *J. Mater. Chem. C*, 4(2016), p. 5962.

[14] D.P. Sun, Q. Zou, G.Q. Qian, C. Sun, W. Jiang, and F.S. Li, Controlled synthesis of porous Fe_3O_4-decorated graphene with extraordinary electromagnetic wave absorption properties, *Acta Mater.*, 61(2013), No. 15, p. 5829.

[15] X.S. Zhang, B. Meng, F.Y. Zhu, W. Tang, and H.X. Zhang, Switchable wetting and flexible SiC thin film with nanostructures for microfluidic surface-enhanced Raman scattering sensors, *Sens. Actuators A*, 208(2014), p. 166.

[16] J.H. Chen, F.M. Zhai, M. Liu, X.M. Hou, and K.C. Chou, SiC nanowires with tunable hydrophobicity/hydrophilicity and their application as nanofluids, *Langmuir*, 32(2016), No. 23, p. 5909.

[17] Y.J. Zhang, J.H. Chen, H.L. Fan, K.C. Chou, and X.M. Hou, Characterization of modified SiC@SiO_2 nanocables/MnO_2 and their potential application as hybrid electrodes for supercapacitors, *Dalton Trans.*, 44(2015), No. 46, p. 19974.

[18] L. Zhang, H.P. Shao, H. Zheng, T. Lin, and Z.M. Guo, Synthesis and characterization of Fe_3O_4@SiO_2 magnetic composite nanoparticles by a one-pot process, *Int. J. Miner. Metall. Mater.*, 23(2016), No. 9, p. 1112.

[19] S.E. Mousavi Ghahfarokhi, S. Hosseini, and M. Zargar Shoushtari, Fabrication of $SrFe_{12-x}Ni_xO_{19}$ nanoparticles and investigation on their structural, magnetic and dielectric properties, *Int. J. Miner. Metall. Mater.*, 22(2015), No. 8, p. 876.

[20] C.H. Gong, J.W. Zhang, C. Yan, X.Q. Cheng, J.W. Zhang, L.G. Yu, Z.S. Jin, and Z.J. Zhang, Synthesis and microwave electromagnetic properties of nanosized titanium nitride, *J. Mater. Chem.*, 22(2012), No. 8, p. 3370.

[21] W.B. Weir, Automatic measurements of complex dielectric constant and permeability at microwave frequencies, *Proc. IEEE*, 62(1974), No. 1, p. 33.

[22] J.H. Chen, W.N. Liu, T. Yang, B. Li, J.D. Su, X.M. Hou, and K.C. Chou, A facile synthesis of a three-dimensional flexible 3C–SiC sponge and its wettability, *Cryst. Growth Des.*, 14(2014), No. 9, p. 4624.

[23] J.H. Chen, Y.J. Zhang, X.M. Hou, L. Su, H.L. Fan, and K.C. Chou, Fabrication and characterization of ultra-light SiC whiskers decorated by RuO_2 nanoparticles as hybrid supercapacitors, *RSC Adv.*, 6(2016), No. 23, p. 19626.

[24] Z.J. Wang, L.N. Wu, J.G. Zhou, W. Cai, B.Z. Shen, and Z.H. Jiang, Magnetite nanocrystals on multiwalled carbon nanotubes as a synergistic microwave absorber, *J. Phys. Chem.* C, 117(2013), No. 10, p. 5446.

[25] Z.S. Wu, S.B. Yang, Y. Sun, K. Parvez, X.L. Feng, and K. Müllen, 3D nitrogen-doped graphene aerogel-supported Fe_3O_4 nanoparticles as efficient electrocatalysts for the oxygen reduction reaction, *J. Am. Chem. Soc.*, 134(2012), No. 22, p. 9082.

[26] T. Pirzada, S.A. Arvidson, C.D. Saquing, S.S. Shah, and S.A. Khan, Hybrid silica–PVA nanofibers via sol–gel electrospinning, *Langmuir*, 28(2012), No. 13, p. 5834.

[27] L.W. Lin, Synthesis and optical property of large-scale centimetres-long silicon carbide nanowires by catalyst-free CVD route under superatmospheric pressure conditions, *Nanoscale*, 3(2011), No. 4, p. 1582.

[28] H.S. Mansur, C.M. Sadahira, A.N. Souza, and A.A.P. Mansur, FTIR spectroscopy characterization of poly (vinyl alcohol) hydrogel with different hydrolysis degree and chemically crosslinked with glutaraldehyde, *Mater. Sci. Eng. C*, 28(2008), No. 4, p. 539.

[29] D.L.A. de Faria, S.V. Silva, and M.T. de Oliveira, Raman

microspectroscopy of some iron oxides and oxyhydroxides, *J. Raman Spectrosc.*, 28(1997), No. 11, p. 873.

[30] X. Huang, J. Zhuang, D. Chen, H. Liu, F. Tang, X. Yan, X. Meng, L. Zhang, and J. Ren, General strategy for designing functionalized magnetic microspheres for different bioapplications, *Langmuir*, 25(2009), No. 19, p. 11657.

[31] K. Kim, M. Kim, J. Kim, and J. Kim, Magnetic filler alignment of paramagnetic Fe_3O_4 coated SiC/epoxy composite for thermal conductivity improvement, *Ceram. Int.*, 41(2015), No. 9, p. 12280.

[32] T. Yoon, C. Chae, Y.K. Sun, X. Zhao, H.H. Kung, and J.K. Lee, Bottom-up *in situ* formation of Fe_3O_4 nanocrystals in a porous carbon foam for lithium-ion battery anodes, *J. Mater. Chem.*, 21(2011), No. 43, p. 17325.

[33] K. Shimoda, J.S. Park, T. Hinoki, and A. Kohyama, Influence of surface structure of SiC nano-sized powder analyzed by X-ray photoelectron spectroscopy on basic powder characteristics, *Appl. Surf. Sci.*, 253(2007), No. 24, p. 9450.

[34] D.P. Sun, Q. Zou, Y.P. Wang, Y.J. Wang, W. Jiang, and F.S. Li, Controllable synthesis of porous Fe_3O_4@ZnO sphere decorated graphene for extraordinary electromagnetic wave absorption, *Nanoscale*, 6(2014), No. 12, p. 6557.

[35] Y.J. Chen, M.S. Cao, T.H. Wang, and Q. Wan, Microwave absorption properties of the ZnO nanowire-polyester composites, *Appl. Phys. Lett.*, 84(2004), No. 17, p. 3367.

[36] X.L. Su, W.C. Zhou, Z.M. Li, F. Luo, H.L. Du, and D.M. Zhu, Preparation and dielectric properties of B-doped SiC powders by combustion synthesis, *Mater. Res. Bull.*, 44(2009), No. 4, p. 880.

[37] Y.J. Chen, P. Gao, C.L. Zhu, R.X. Wang, L.J. Wang, M.S. Cao, and X.Y. Fang, Synthesis, magnetic and electromagnetic wave absorption properties of porous $Fe_3O_4/Fe/SiO_2$ core/shell nanorods, *J. Appl. Phys.*, 106(2009), No. 5, art. No. 054303.

[38] Y.J. Chen, G. Xiao, T.S. Wang, Q.Y. Ouyang, L.H. Qi, Y. Ma, P. Gao, C.L. Zhu, M.S. Cao, and H.B. Jin, Porous Fe_3O_4/carbon core/shell nanorods: synthesis and electromagnetic properties, *J. Phys. Chem. C*, 115(2011), p. 10061.

[39] Y.J. Chen, F. Zhang, G.G. Zhao, X.Y. Fang, H.B. Jin, P. Gao, C.L. Zhu, M.S. Cao, and G. Xiao, Synthesis, multi-nonlinear dielectric resonance and excellent electromagnetic absorption characteristics of Fe_3O_4/ZnO core/shell nanorods, *J. Phys. Chem. C*, 114(2010), No. 20, p. 9239.

[40] M.S. Cao, J. Yang, W.L. Song, D.Q. Zhang, B. Wen, H.B. Hou, Z.L. Yuan, and J. Yuan, Ferroferric oxide/multiwalled carbon nanotube vs polyaniline/ferroferric oxide/multiwalled carbon nanotube multiheterostructures for highly effective microwave absorption, *ACS Appl. Mater. Interfaces*, 4(2012), No. 12, p. 6949.

[41] S.S. Kim, S.B. Jo, K.I. Gueon, K.K. Choi, J.M. Kim, and K.S. Churn, Complex permeability and permittivity and microwave absorption of ferrite-rubber composite at X-band frequencies, *IEEE Trans. Magn.*, 27(1991), No. 6, p. 5462.

[42] S.C. Chiu, H.C. Yu, and Y.Y. Li, High electromagnetic wave absorption performance of silicon carbide nanowires in the gigahertz range, *J. Phys. Chem. C*, 114(2010), No. 4, p. 1947.

[43] H.J. Yang, M.S. Cao, Y. Li, H.L. Shi, Z.L. Hou, X.Y. Fang, H.B. Jin, W.Z. Wang, and J. Yuan, Enhanced dielectric properties and excellent microwave absorption of SiC powders driven with NiO nanorings, *Adv. Opt. Mater.*, 2(2014), No. 3, p. 214.

[44] S. Xie, G.Q. Jin, S. Meng, Y.W. Wang, Y. Qin, and X.Y. Guo, Microwave absorption properties of *in situ* grown CNTs/SiC composites, *J. Alloys Compd.*, 520(2012), p. 295.

[45] R.B. Yang, P.M. Reddy, C.J. Chang, P.A. Chen, J.K. Chen, and C.C. Chang, Synthesis and characterization of Fe_3O_4/polypyrrole/carbon nanotube composites with tunable microwave absorption properties: Role of carbon nanotube and polypyrrole content, *Chem. Eng. J.*, 285(2016), p. 497.

[46] Z.J. Wang, L.N. Wu, J.G. Zhou, B.Z. Shen, and Z.H. Jiang, Enhanced microwave absorption of Fe_3O_4 nanocrystals after heterogeneously growing with ZnO nanoshell, *RSC Adv.*, 3(2013), p. 3309.

[47] L.G. Yan, J.B. Wang, X.H. Han, Y. Ren, Q.F. Liu, and F.S. Li, Enhanced microwave absorption of Fe nanoflakes after coating with SiO_2 nanoshell, *Nanotechnology*, 21(2010), No. 9, art. No. 095708.

[48] C.C. Lee and C.H. Chen, Ag nanoshell-induced dual-frequency electromagnetic wave absorption of Ni nanoparticles, *Appl. Phys. Lett.*, 90(2007), No. 19, art. No. 193102.